Engineering Fracture Mechanics xxx (2017) xxx–xxx

Contents lists available at ScienceDirect

Engineering Fracture Mechanics

journal homepage: www.elsevier.com/locate/engfracmech

A practical approach to modeling aluminum weld fracture for structural applications

P.B. Woelke [a,*], B.K. Hiriyur [a], K. Nahshon [b], J.W. Hutchinson [c]

[a] Weidlinger Applied Science, Thornton Tomasetti, Inc., New York, NY, United States
[b] Survivability, Structures, Materials, and Environmental Department, Naval Surface Warfare Center Carderock Division, West Bethesda, MD, United States
[c] School of Engineering and Applied Sciences, Harvard University, Cambridge, MA, United States

ARTICLE INFO

Article history:
Received 24 July 2016
Received in revised form 9 February 2017
Accepted 13 February 2017
Available online xxxx

Keywords:
Welded aluminum
Undermatched welds
Ductile fracture
Large scale structures
Cohesive zone
Shell elements

ABSTRACT

This paper addresses the numerical simulation of plasticity and ductile fracture of large scale structures (e.g. ships, railcars, automobiles) fabricated with welds that exhibit appreciably lower strength than the plate material, often referred to as weld undermatching. It has been observed, both numerically and experimentally, that for such structures the weld undermatching often leads to plasticity and fracture being limited to the weld and heat affected zone (HAZ). While the large size of the structures of interest precludes the use of a refined three-dimensional element mesh capable of capturing the details of the weld/HAZ behavior, cohesive zones are ideal for capturing the overall effects of undermatched weld plasticity and fracture on a structural scale. This paper focuses on establishing a systematic calibration process for determining the cohesive zone constitutive behavior and examining the validity of this approach in the context of mode I tearing of a large welded two-layer AA6061-T6 sandwich panel. First, test data from a welded coupon is used to calibrate the cohesive law. Tearing fracture of this panel is examined using the established cohesive law to represent weld/HAZ along with elastic-plastic shell elements, with in-plane dimensions much greater than the layer thickness, to represent the parent metal. It was verified that, for this structure, plasticity was indeed confined to the welds and heat affected zones, and that the behavior of the panel was captured with reasonable fidelity.

1. Introduction

Structural aluminum alloys possess several properties that make their use desirable for a variety of structures. In particular, transportation structures (e.g. ships, aircraft, trains, and automobiles) utilize the high strength-to-weight ratio, ductility and corrosion resistance to improve vehicle efficiency and performance. One problem area for aluminum structures is the reduced strength of welded connections—the welding process involves local heating of the metal resulting in a local strength reduction in the weld and/or in the region immediately adjacent to the weld, referred to as the heat affected zone (HAZ). Often, fracture initiates and remains in this weakened HAZ rather than the parent or base metal (BM). This local strength reduction, referred to as undermatching, results in welded joints largely controlling the structural failure of welded aluminum structures. Furthermore, the quality of aluminum welds is highly sensitive to the weld fabrication technique. Thus,

* Corresponding author.
E-mail address: pwoelke@thorntontomasetti.com (P.B. Woelke).

http://dx.doi.org/10.1016/j.engfracmech.2017.02.010
0013-7944/

Nomenclature

T	nominal cohesive traction
δ	cohesive separation
$T(\delta)$	traction-separation relation
$\hat{T}$ peak	cohesive traction
t	plate thickness
$\delta_1, \ldots, \delta_n, \delta^F$	traction-separation relationship shape parameters
Γ	cohesive energy/area
Δx	distance ahead of the pre-crack
$\Gamma(\Delta x)$	cohesive energy/area as functions of distance Δx ahead of the pre-crack
E	elastic modulus
n	hardening exponent
σ	trues stress
ε	trues strain
σ_y	yield stress
$\Gamma_{ss-weld}$	steady-state tearing energy of the weld/HAZ
Γ_{ss}	steady-state cohesive energy
t	thickness

even for combinations of aluminum alloy and welding process that minimize the reduction of strength in the weld/HAZ, it is common to see fracture occur purely in the welded region due to manufacturing defects.

An important characteristic of undermatched welds is that, with sufficient undermatching, the development of large-scale plasticity as a means of energy dissipation may be curtailed as plastic straining tends to localize in the weld region (e.g. Liu et al. [10], Sutton et al. [29], Wang et al. [38,39]). Thus, undermatched weld properties must be accounted for in the design process likely resulting in a significant weight penalty. For transportation structures, this weight penalty comes at a cost to system level performance including crashworthiness, weight, fuel economy, etc.

For reasons of computational efficiency, the only feasible way to model plasticity and fracture of large-scale structures and structural components with length scale on the order of several to tens of meters is to use shell finite elements with the in-plane dimension larger than the shell thickness (Kõrgesaar and Romanoff [8], Voyiadjis and Woelke [35,36], Woelke et al. [40–42,44–47]). The intention of this paper is to present a simulation methodology for weld fracture in large-scale aluminum plate and shell structures having long linear welded joints under predominantly tensile loading conditions. The proposed methodology exploits the existence of appreciable weld undermatching resulting in the majority of the plastic dissipation and fracture occurring in the weld and/or HAZ. Such behavior can be well represented by a finite element model where a cohesive zone is used to capture necking, localization and fracture in the weld/HAZ and large elastic-plastic shell elements are used to simulate deformation in the parent metal.

This approach has many parallels with the previous investigation by Woelke et al. [42], where mode I crack growth in a large monolithic Al5083-H116 plate under large scale yielding was simulated. A cohesive zone was used to represent necking, localization and fracture at the scale of the plate thickness (and below), while large shell elements were used to model the deformation of the plate away from the crack. This allowed separation of the work of the fracture processes, including necking, from the plastic work dissipated in the surrounding field. This recent paper can in turn be considered a continuation of the early simulation of mode I crack growth under small scale yielding plane strain conditions performed by Tvergaard and Hutchinson [31]. Other contributions relevant to the current work include efforts to simulate aluminum spot weld failure using cohesive zone by Cavalli et al. [4] as well as Zhou et al. [53,54]. Behavior of spot welds is however quite different than continuous linear welds, mainly due to different levels of constraint. An important aspect of the work by Cavalli et al. is the use of fully annealed work-hardenable alloy Al5754-O for which fusion joints will not exhibit material strength degradation in the HAZ. The focus of the current work is on significantly undermatched welds, which in most cases causes plastic dissipation to be confined to the weld and/or HAZ regions.

The main objective of this paper is not on development of a general numerical modeling capability based on use of a cohesive zone. Rather, the main focus is on addressing a specific problem of undermatched weld fracture in large-scale structures, thereby demonstrating that a method employing a properly calibrated cohesive zone is ideally suited for modeling tearing fracture of plate and shell structures with linear undermatched welds. We refer to the proposed procedure as the Welded Aluminum Fracture Modeling Method (WALFRAM). While the present interest is in aluminum structures, we note that any metal that derives its strength from quenching will likely undergo local annealing during welding, which may result in significant weld undermatching. For example, hot-stamped martensitic steels exhibit such behavior during welding, as evidenced by significant (~35–40%) hardness reduction in the HAZ comparing to the base metal (Banik et al. [3]). In addition,

Please cite this article in press as: Woelke PB et al. A practical approach to modeling aluminum weld fracture for structural applications. Engng Fract Mech (2017), http://dx.doi.org/10.1016/j.engfracmech.2017.02.010

highly undermatched weld filler materials are often utilized for high-strength steels and such weldments exhibit similar mechanical behavior to aluminum welds (e.g. Hao et al. [6]). The proposed modeling approach is applicable to all weld fracture problems where significant weld undermatching exists.

The aluminum fracture weld modeling approach discussed here has been successfully integrated into the process of modeling and simulation-based qualification of full-scale ship structures by the authors of this work.

In order to motivate and validate this approach, the paper begins with a brief discussion of the mechanism of weld undermatching in Section 2. Next, a brief discussion of the cohesive zone model and initial calibration using a single welded coupon is provided in Section 3. In Section 4 the modeling approach is exercised for a large welded component with further discussion of the calibration process for the cohesive zone. The analysis results demonstrate the validity of the assumptions and modeling methodology. Concluding remarks and discussion of future work are given in Section 5.

2. Characteristics of welded aluminum

2.1. Aluminum strengthening and welding

The basic state of high purity aluminum is an annealed condition that exhibits low yield strength and high ductility. Producing a structural aluminum alloy requires strengthening which typically also reduces the ductility. Strengthening can be achieved by solid solution hardening followed by precipitation hardening and heat treatment for heat-treatable alloys (e.g. 2xxx, 6xxx, 7xxx series) or cold working for work-hardened alloys (e.g. 5xxx series). A typical heat treatment involves heating to 450–530 °C (depending on the alloy) followed by quenching to obtain supersaturated solid solution. Quenching can be achieved by cooling in water, oil, air or salt-bath, and it produces high strength and lower ductility material. To improve the ductility and formability, the material is aged at room temperature (i.e. natural aging) or at elevated temperature (i.e. artificial aging). The aging temperature and time depend on the alloy and desired properties. The work-hardened alloys derive their strength primarily from cold working, which is achieved by rolling or tractioning of structural shapes (Mazzolani [13]). Similarly to heat treatment, cold working leads to increased strength and reduced ductility.

Heating the aluminum alloy to the temperature of 200–350 °C or higher, which occurs during welding, tends to reverse the effects of heat treatment or cold working, returning the alloy to its original state. In the case of non-heat-treatable alloys, this is basically an annealed condition (lower strength and higher ductility). Welding the heat-treatable alloys typically reduces their strength to a level slightly above the annealed condition. This is illustrated in Fig. 1 [7].

Fig. 1 indicates that welding can lead to approximately 20% strength reduction for non-heat-treatable alloys, and almost 40% for heat-treatable alloys. From the point of view of fracture toughness, the strength reduction is often offset by significant increase in ductility. The loss of strength leads to localization of the plastic deformation in the weld and/or HAZ, which has a profound consequence for behavior of welded aluminum structures. As previously noted, similar behavior is observed in martensitic steels.

2.2. Aluminum weld strength profile

The material in the vicinity of a typical aluminum weld can be characterized by three regions of differing strength and ductility: weld metal (WM); heat affected zone (HAZ); and unaffected base material (BM) (Zheng et al. [51]). Aluminum welds typically feature a gradient of grain structure that results in varying mechanical properties within the HAZ itself. Fur-

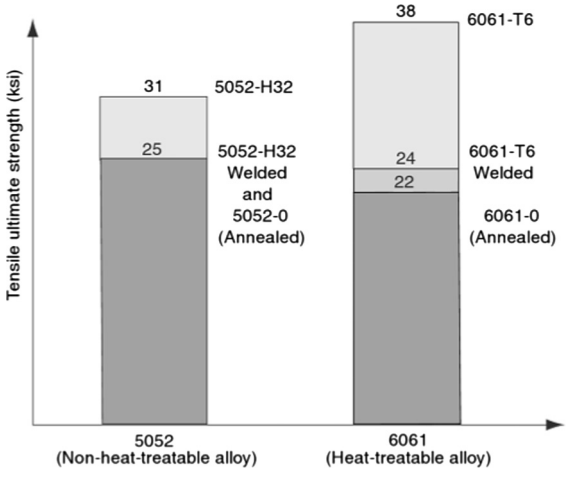

Fig. 1. Effect of welding on tensile ultimate strength of alloys 5052 and 6061 (reproduced from Kissel and Ferry [7]).

Please cite this article in press as: Woelke PB et al. A practical approach to modeling aluminum weld fracture for structural applications. Engng Fract Mech (2017), http://dx.doi.org/10.1016/j.engfracmech.2017.02.010

thermore, in certain welds distinct sub-regions exist where mechanical properties are lowest. Several means of characterizing the material in these regions have been proposed. The most common test is the Vickers hardness test which is used to provide a profile of the weld strength at various distances from the weld center. Hardness is a measure of resistance to penetration which can be directly related to ultimate stress for many alloys (Baker [2], Tabor [30]). While hardness measurements are straightforward surface measurements typically associated with significant scatter, they provide a simple and effective method of approximate determination of material strength distribution. A sample hardness map of a 5083-H116 Metal Inert Gas (MIG) weld along with microstructural images of various regions of this weld are shown in Fig. 2. The hardness profile clearly indicates significant strength reduction in the weld and heat affected zone. The microstructural images show a corresponding change in the grain structure: cold-work-induced grain orientation (or texture) is visible in the unaffected plate (top right image) and loss of the orientation resulting from local heating is visible in the HAZ (bottom right image).

Material hardness can be closely correlated to strength for many heat-treatable alloys. However, the hardness test does not provide detailed stress-strain characterization for the materials in various regions of the weld. To obtain such data, tensile testing on miniature specimens extracted from the weld zone can be performed, as shown by Matusiak [12], as well as Negre et al. [17,18]. Miniature tensile specimens can be problematic due to sensitivity to local porosity and defects in the weld zone, commonly observed in aluminum fusion welds. Alternatively, Digital Image Correlation (DIC) techniques (e.g. Reynolds and Duvall, [25]) or closely-spaced strain gauges (e.g. Zheng et al. [51]) can be used to obtain in-situ surface strain measurements. These measurements can be used to extract uniaxial stress-strain data at various locations. Fig. 3 shows local stress-strain data obtained through DIC for the weld shown in Fig. 2. We note that Vickers hardness tests correspond to a strain level of approximately 7%.

2.3. Plastic strain localization

The weld hardness profile illustrated in Fig. 2 is typical of aluminum welds in various alloys. While different welding techniques (friction stir welding, laser beam welding) and quality control can produce significant variations of the hardness profiles (e.g. Li & Chandra [9], Liu et al. [11], Negre et al. [17,18]), it is generally observed that both the weld and the HAZ are weaker than the base material. Consequently, behavior of the welded aluminum components is controlled by the welded joint, with plastic deformation localizing in the region of reduced strength.

For cases where the degree of undermatching is sufficient, the base metal remains elastic while the material in the HAZ and/or WM yields and deforms plastically to high levels of strain. An example of this behavior was discussed by Zheng et al. [51] who investigated a 6061-T6 aluminum weld and showed that localization and fracture were controlled by the course grained part of the heat affected zone (CGHAZ). Further tests of a structural panel with this same weld joint reported by

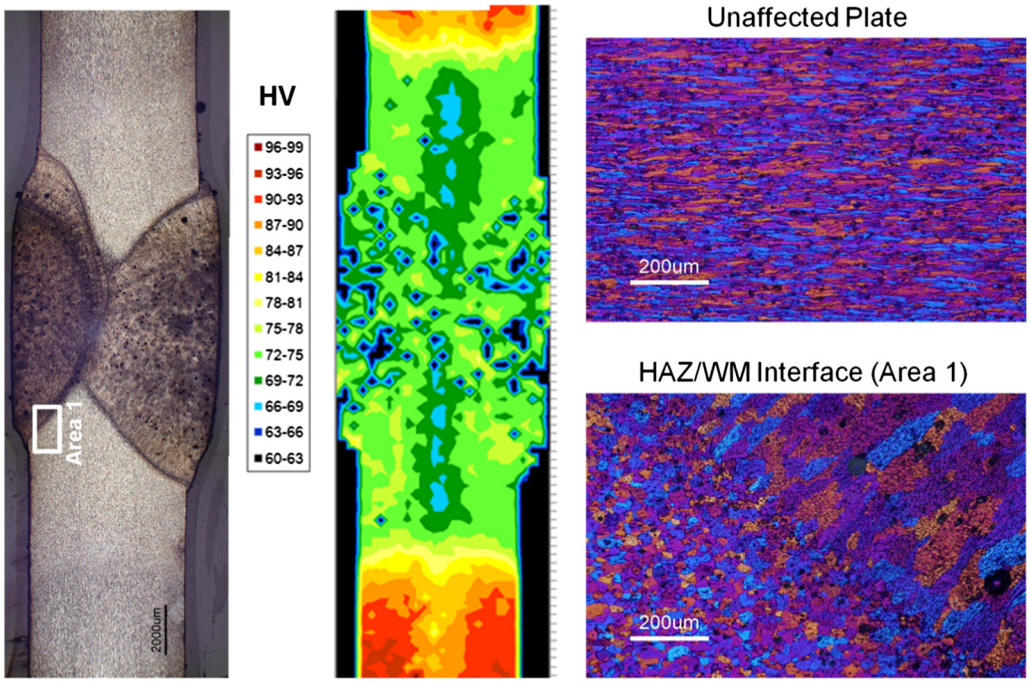

Fig. 2. Hardness map showing the different material zones for a typical MIG weld joint in 5083-H116. A dramatic change in microstructure and hardness is exhibited in the HAZ as compared to the unaffected parent plate (Nahshon & Zok [14]).

Please cite this article in press as: Woelke PB et al. A practical approach to modeling aluminum weld fracture for structural applications. Engng Fract Mech (2017), http://dx.doi.org/10.1016/j.engfracmech.2017.02.010

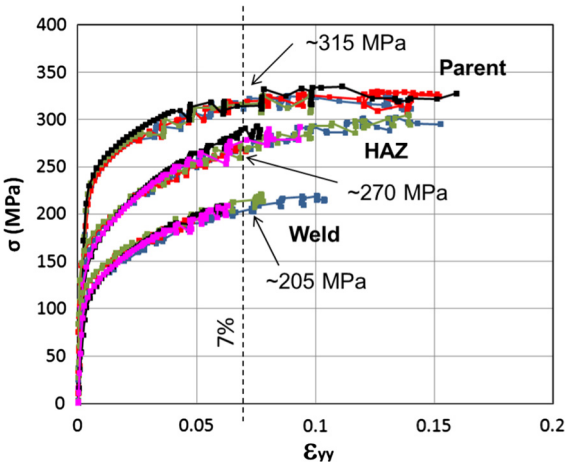

Fig. 3. Local tensile stress-strain characterization in a typical MIG weld joint. The local tensile specimens were extracted in situ via DIC from different locations of the same welded joint (Nahshon & Zok [14]).

Zheng et al. [50] illustrated the controlling effect that severe undermatching had on overall structural performance. An analysis of this test series is presented in Section 4 of this paper.

Although welding causes strength reduction of the HAZ in reference to the base metal, it is accompanied by an increase in ductility (since welding returns material to, or near, the annealed state). As a result, the HAZ can actually have higher tearing toughness than the parent metal. Nevertheless, low strength tends to confine the extent of plastic deformation to the welded joint, which negatively affects the overall effective toughness of the structure by reducing overall plastic dissipation. This behavior can be detrimental to the ultimate load carrying capacity and overall toughness of welded aluminum structures. In conclusion, significant weld undermatching may result in *crack initiation and propagation in the weld/HAZ joint with negligible plasticity outside the joint*. Since the crack path is predictable for such situations, this class of welded structures is well suited for simulation using the cohesive zone methodology. Moreover, the weld undermatching and resulting assumption about localization of plasticity in the weld and HAZ, allows development of a simple and systematic calibration process for the traction-separation relationship. Somewhat paradoxically, weld undermatching simplifies prediction of plasticity and fracture on a structural scale. The approach used in this paper employs elastic-plastic shell elements to model the base material in the plates in order to capture plasticity outside the welded joint if it does occur.

An alternative methodology to modeling undermatched welds would be to treat weld and HAZ as separate materials that are explicitly represented by means of the same type of elements used to model the base material (e.g. Nielsen et al. [20,21], Rashid and Tvergaard [24], Wadley et al. [37], Wang et al. [38,39], Zheng et al. [49–51]). This approach requires the element size to be smaller than the weld/ HAZ. Depending on the discretization level, the behavior of the weld and specific regions within the HAZ (including softening and failure) can be represented as different materials [38,39] or the weld and HAZ can be represented as one material with effective reduced properties. In the former case, relatively small three-dimensional elements would be required to explicitly model the constituent materials (including the weld nugget, CGHAZ, FGHAZ, etc.). The latter approach is often referred to as the weakened element approach. One of the key advantages of the cohesive zone methodology is the fact that it employs the effective work of separation per unit area of the welded joint – a mesh independent quantity. In contrast, the weakened element approach, where the weakened elements represent nonlinear deformation and failure of the weld/HAZ, inherently depends on the length scale (i.e. mesh size) used in discretizing the reduced strength zone.

3. Cohesive zone model and initial calibration

3.1. Cohesive zone model

Cohesive zone models have been widely employed for fracture problems (e.g. Anvari et al. [1], Needleman [16], Ortiz & Pandolfi [23], Scheider & Brocks [26], Tvergaard and Hutchinson [32], Woelke et al. [41–43]). They are particularly well suited for problems where the crack path is predictable, such as delamination problems (e.g. Sills and Thouless [27], Tvergaard and Hutchinson [33], Woelke et al. [43], Yang and Thouless [48]) or weld fracture (e.g. Cavalli et al. [4] as well as Zhou et al. [53,54]). The cohesive zone is characterized by the traction-separation relation, which defines the relationship between the cohesive tractions and the separation of the crack faces.

As already emphasized, the weld fracture methodology developed herein is intended for large-scale welded aluminum plate and shell structures which can only be effectively modeled by plane stress plate/shell elements with in-plane dimensions larger than the plate/sheet thickness (as opposed to solid elements that are small compared to the thickness, e.g. Niel-

Please cite this article in press as: Woelke PB et al. A practical approach to modeling aluminum weld fracture for structural applications. Engng Fract Mech (2017), http://dx.doi.org/10.1016/j.engfracmech.2017.02.010

sen [19]). Explicit representation of the through-thickness behavior of the different materials in the welded joint (i.e. BM, WM, HAZ) requires a level of discretization that is only practical for relatively small welded coupons. Thus, in the present approach the cohesive zone is calibrated to model the *overall separation behavior of the joint* while the base material outside the joint is modeled with standard shell elements (Fig. 4). The cohesive zone is defined by traction calculated as force/length, versus separation (or end displacement) obtained directly from an experiment on a specimen gauge length that includes the weld and heat effected zone. The goal is to effectively calibrate the cohesive zone such that it reproduces the strength and energy dissipation due to yield and separation failure of the combined weld/HAZ region. We note that the force/length-separation could also be obtained from a detailed numerical simulation of the gauge section. However, this would require significantly higher level of discretization as well as large strain formulation along with advanced constitutive model that incorporates damage and failure. The 'beauty', or perhaps one should say 'practicality' of the present approach from an engineering point of view, is that the force/length-displacement relation of the cohesive law can be accurately specified within the small strain framework. This is because all the large strain behavior is captured within the representative behavior of the gauge length and everything outside the cohesive zone is accurately represented by small strain behavior.

In the current paper, we focus on mode I separations normal to the weld direction (Fig. 4). In-plane and out-of-plane shear modes (mode II and III) are not considered. Thus, only in-plane translational degrees of freedom normal to the weld are governed by cohesive zone. The remaining degrees of freedom, including rotations are free on both sides of the cohesive zone.

The traction-separation relation, $T(\delta)$, along with the schematic representation of the welded aluminum specimen such a test coupon are given in Fig. 4. The peak traction, $\hat{T}$, and the parameters, $\delta_1, \ldots, \delta_n$ and δ^F determine the shape of the traction-separation. As discussed by the authors in [42], these parameters as well as the cohesive energy/area, $\Gamma(\Delta x)$ can be regarded as functions of distance Δx ahead of the pre-crack or notch if the calibration process dictates such dependency.

The implementation of the cohesive zone model used in the current study is based on one-dimensional spring-type elements connecting two nodes on the opposite side of the weld. The traction-separation can be input as a general, piecewise-linear curve with any number of pairs of (T, δ). This corresponds to a set of shape parameters, i.e. $\delta_1, \delta_2, \ldots, \delta_n, \delta^F$. The cohesive energy/area is given by:

$$\Gamma(\Delta x) = \int_0^{\delta^F} T d\delta \tag{1}$$

While plane strain studies [31] have indicated that the two most important properties of the traction-separation law are the peak traction and the energy of separation, more recent investigation by the authors [42] indicated some sensitivity of the response to the details of the shape parameters for applications similar to those considered here. The influence of the shape of the traction-separation law was also investigated by Hachez [5], Sills and Thouless [27], Volokh [34] and other authors, who indicated that the shape may have significant influence, depending on the application.

3.2. Welded coupon tensile test and initial calibration of the traction-separation relationship

An extensive experimental program involving both coupon and component level welded aluminum specimens subjected to mode I and mode III loading was conducted by Zhang et al. [49–51]. In the current paper, we focus on the mode I fracture test of the large scale welded AA 6061 extrusion [50], discussed in Section 4, along with the corresponding coupon level test [51] used in this section for calibration of the cohesive traction-separation relationship.

The plastic part of the true stress-logarithmic strain response of this material was approximated by the following power law relationship: $\sigma = 328.7(\varepsilon^{0.06})$, as shown in Fig. 5.

A welded tensile specimen made of the same material with a friction stir weld in the center was tested to characterize the weld behavior. The welded specimen dimensions as well as its finite element representation are shown in Fig. 6. The spec-

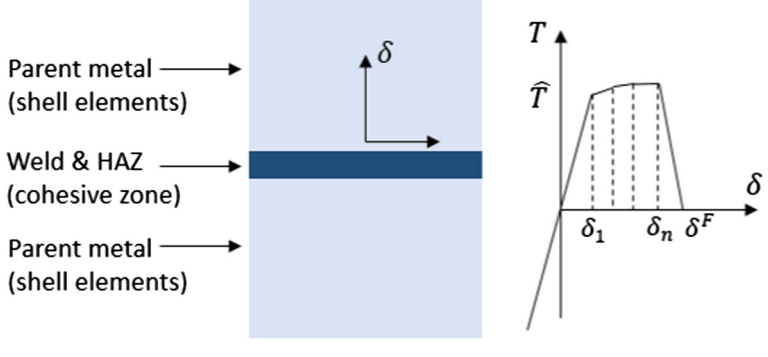

Fig. 4. Schematic representation of the welded aluminum component and general traction-separation relationship with peak traction $\hat{T}$ and shape parameters, $\delta_1, \ldots \delta_n$ and δ^F.

Please cite this article in press as: Woelke PB et al. A practical approach to modeling aluminum weld fracture for structural applications. Engng Fract Mech (2017), http://dx.doi.org/10.1016/j.engfracmech.2017.02.010

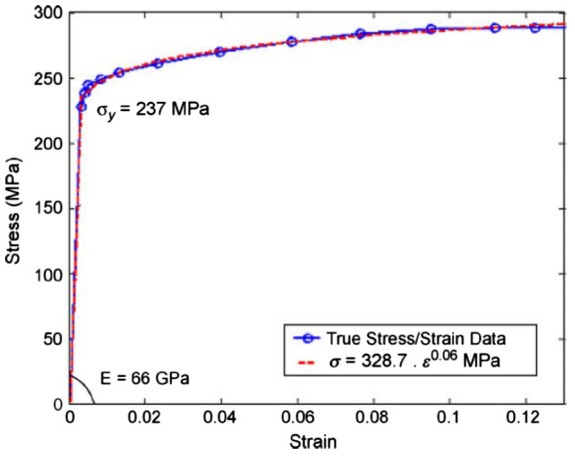

Fig. 5. True stress-strain response of the base metal AA 6061, including the formula fitting the data (reproduced from Zheng et al. [52]).

imen was designed to represent the welded joint in the large scale mode I fracture test of the extruded structural panel discussed in the next section. It has the same thickness (3.2 mm) as the plates comprising the panel. The width of the specimen at the weld is slightly more than 4 times the plate thickness and can be expected to produce conditions of approximately plane strain tension after plastic flow begins in the weld, similar to the conditions of a long linear weld undergoing mode I tearing. The force-load point displacement curve measured for the specimen is given in Fig. 7(a). The abrupt force drop terminating the test entails shear localization and shear-off which consumes very little energy.

The coupon test was modeled using large shell elements with an average in-plane dimension of 7 mm (2 × the sheet thickness) representing the parent metal. The material parameters used in the analysis were as follows: $E = 66$ GPa, $\sigma_y = 237$ MPa, $n = 0.06$; where n is the hardening exponent. The comparison of the measured and calculated force-displacement response, as well as the contour plots of axial displacements and equivalent plastic strains are shown in Fig. 8.

The analysis of the coupon test confirmed that the response outside the welded joint was entirely elastic. Fig. 7 illustrates the straightforward manner in which the cohesive response of the joint is identified. The elastic response of the full specimen, including the weld, is shown in Fig. 7(b). The portion of the response attributed to the cohesive zone in Fig. 7(c) is the difference between the total response in Fig. 7(a) and the linear response in Fig. 7(b). The small elastic response arising from the weld is included in the plate elements. With T identified as the force divided by the initial cross-sectional area of the gauge section ($\hat{T} \cong 200$ MPa) and δ as the displacement in Fig. 7(c), the separation energy Γ is defined by (1). This value, $\Gamma_{ss-weld} = 831$ kJ/m^2, is assumed to govern the steady-state tearing energy of the weld/HAZ applicable after the crack has

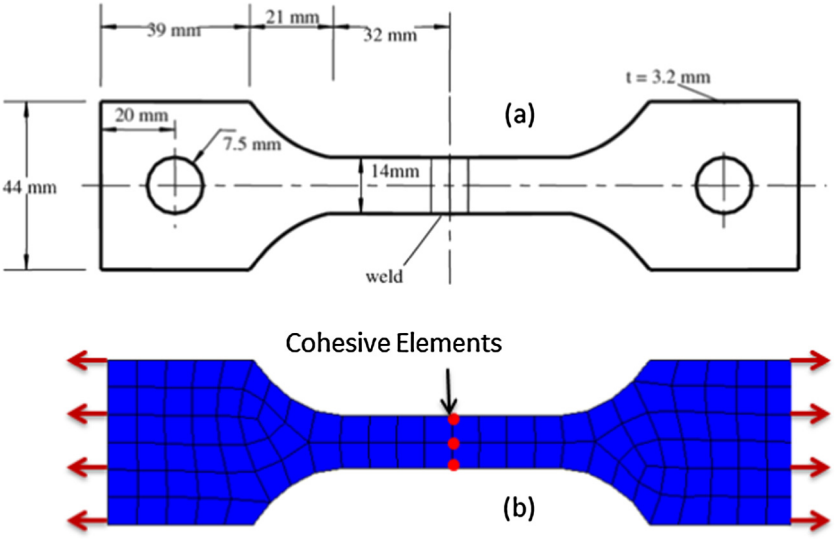

Fig. 6. Welded tensile specimen [51] and its finite element representation

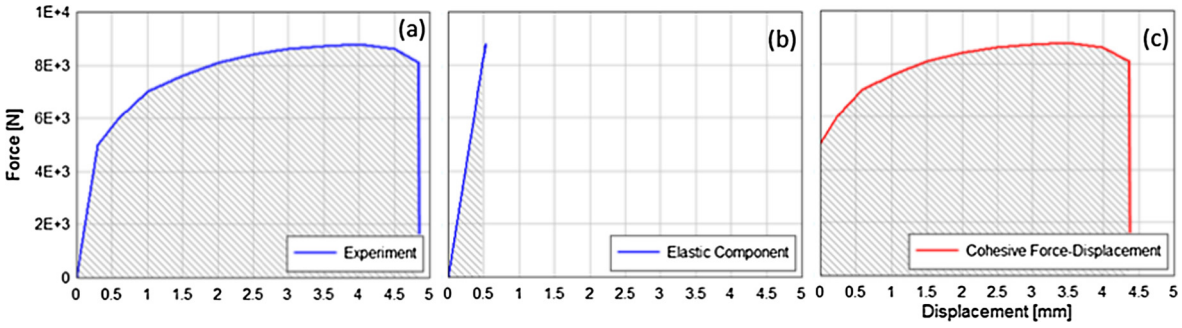

Fig. 7. Decomposition of force-displacement and strain energy into the elastic and plastic contributions for the welded coupon test: (a) Total force-displacement and strain energy [51]; (b) Elastic contribution to force-displacement and strain energy; (c) Plastic contribution to force-displacement and strain energy (note that $\delta_n \approx \delta^F$).

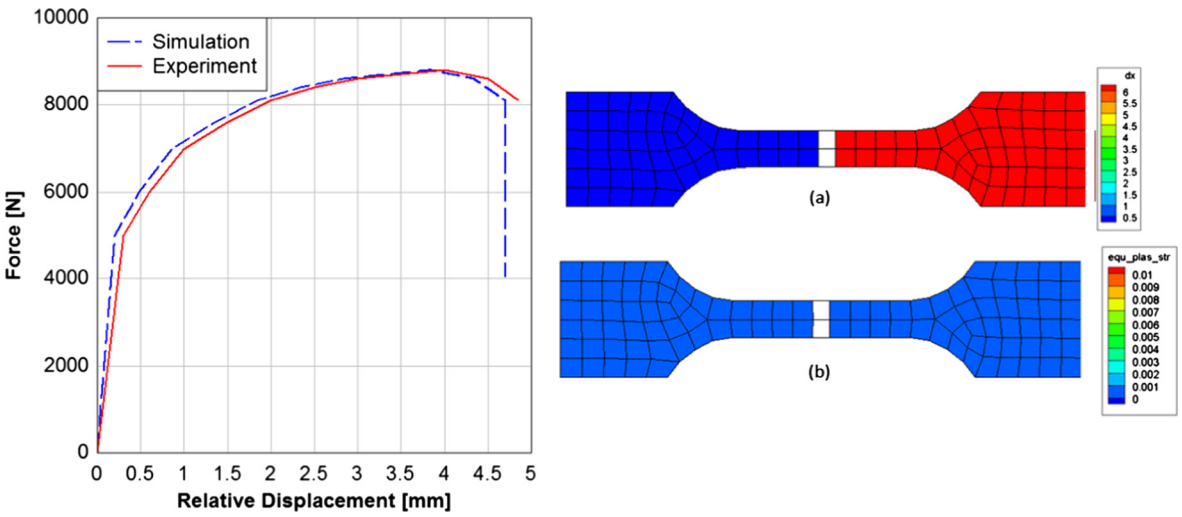

Fig. 8. Comparison of the measured and calculated force-displacement response for a tensile welded aluminum coupon and contour plots of the calculated displacements and equivalent plastic strains at peak traction.

advanced at least several plate thicknesses. The possibility that the separation energy depends on the distance ahead of the initial crack tip in the initial stages of crack growth will be addressed in the next section in a second iteration of the calibration process. As expected, by employing the cohesive law $T(\delta)$ derived from Fig. 7(c) in a simulation of the coupon specimen, one reproduces the overall force-displacement response seen in Fig. 7 and confirms that the plate elements outside the welded joint remain in the elastic range.

4. Mode i fracture of large welded aluminum extrusion

4.1. Experimental test of large welded aluminum extrusion

The mode I test of a large welded two-layer extruded AA 6061 sandwich plate (Zhang et al. [50]) is investigated here. The test specimen was built by friction-stir-welding two extrusions on both sides, along the length of the specimen (except for the pre-notch region), as shown in Figs. 9 and 10(a). The tested extrusions included rails for train equipment attachment (e.g. seats). These rails did not affect the overall behavior of the panels, as shown by Zhang et al. [49–51], and were therefore not considered here. These welded panels were subjected to mode I tension as shown in Figs. 9 and 10(a). Fig. 10 provides the dimensions of the specimen, the loading direction and overall force-displacement responses measured from two nominally identical tests.

The test discussed above bears certain resemblance to another mode I fracture test of a large unwelded Al5083-H116 plate of 10 mm thickness conducted by Simonsen and Törnqvist [28]. The details of the necking and slant fracture observed in the Simonsen-Tornqvist test during the phase of steady-state propagation were investigated by Nielsen and Hutchinson [22] utilizing a shear-modified Gurson model [15]. Findings of this investigation were later used by Woelke et al. [42] to sim-

Please cite this article in press as: Woelke PB et al. A practical approach to modeling aluminum weld fracture for structural applications. Engng Fract Mech (2017), http://dx.doi.org/10.1016/j.engfracmech.2017.02.010

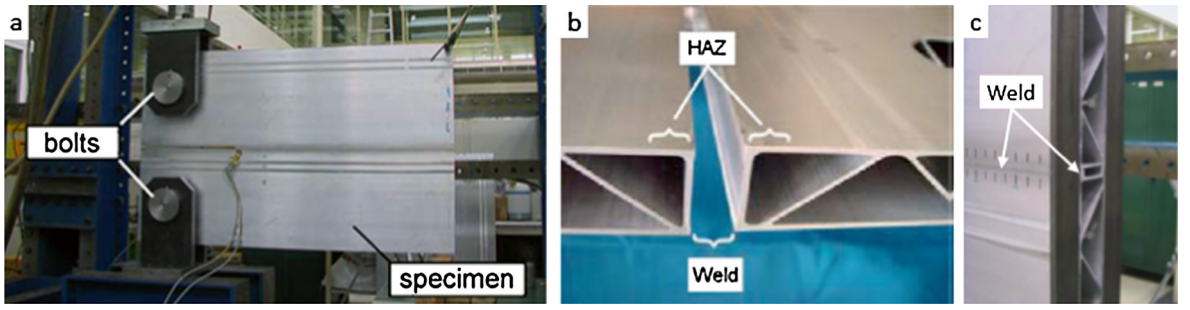

Fig. 9. Mode I fracture test of a welded aluminum extrusion: (a) the experimental setup for mode I testing of large panels – welded train extrusion; (b) the cross section of the extrusion showing the two welded sides with weld and HAZ regions; (c) the back side of the panel showing the weld region (reproduced from Zheng et al. [50]).

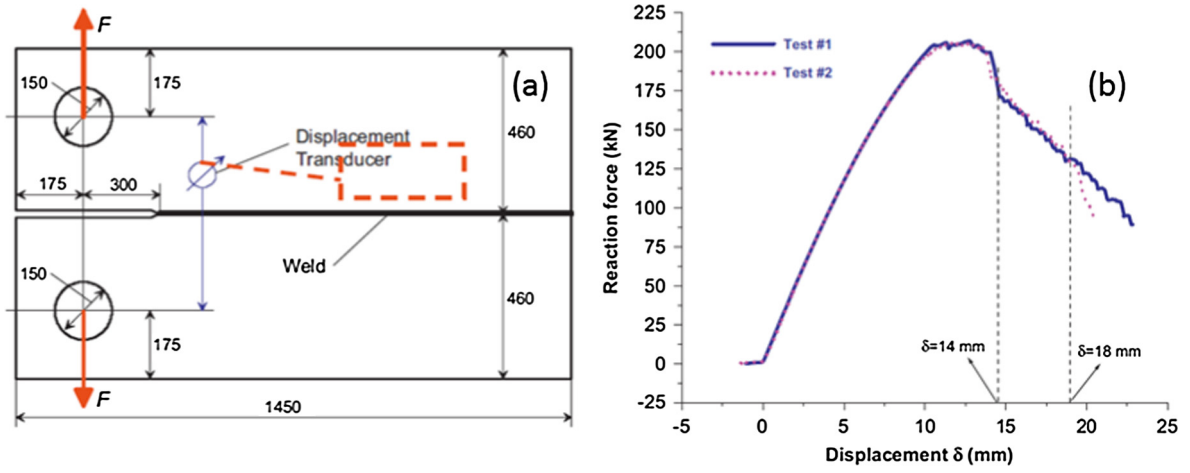

Fig. 10. (a) Schematic of test setup and (b) Force-displacement results for Mode I fracture test of a welded aluminum extrusion (reproduced from Zheng et al. [50]).

ulate full crack propagation in the same plate using a similar approach to the one discussed in this paper (i.e. large shell elements and cohesive zone). The steady-state crack growth resistance calculated in [20] was used to characterize the steady-state cohesive energy, which was achieved after the after crack had advanced 6–7 plate thicknesses. The investigation revealed that the steady-state cohesive energy ($\Gamma_{ss} = 1175$ kJ/m^2), was approximately 35 times the cohesive energy necessary to initiate the crack from a blunt notch tip. Such behavior is consistent with the fact that a fully developed necking zone ahead of the crack tip requires the crack tip to advance at least several plate thicknesses. It is the necking which contributes most of the energy dissipated by the cohesive zone. To model the history of crack advance and the overall load-displacement behavior in the Al5083-H116 plate from initiation to steady-state it was essential to account for the x-dependence of the cohesive zone energy. Furthermore, in the case of the unwelded Al5083-H116 plate, the majority of plastic dissipation (~66%) occurred outside the cohesive zone associated with large-scale yielding. These findings will serve as a reference for the case considered here. In particular, whether the weld considered in the present paper has a similar x-dependence of its cohesive energy is investigated in this section as the second iteration of the calibration process.

4.2. Simulation of the mode I fracture of large welded aluminum extrusion

The welded extrusion simulations model was built using quadrilateral shell elements with the average in-plane dimension of 21 mm. As previously noted, nodal cohesive elements placed on both sides of the extrusion, along the length of the weld were used to simulate the weld and HAZ, as shown in Fig. 11. The model was restrained laterally and vertical velocity boundary conditions were applied along the bolt holes to model the mode I tensile loading shown in Figs. 9 and 10.

The traction-separation relation determined through the analysis of the welded coupon discussed in the previous section serves as a basis for cohesive elements used here, at least after the crack has undergone sufficient extension. The cohesive energy obtained from the welded coupon test (shaded zone in Fig. 7(c), normalized by the cross-sectional weld area) gives the steady state cohesive energy/area: $\Gamma_{ss-weld} = 831$ kJ/m^2. The first simulation has been carried out using an x-independent

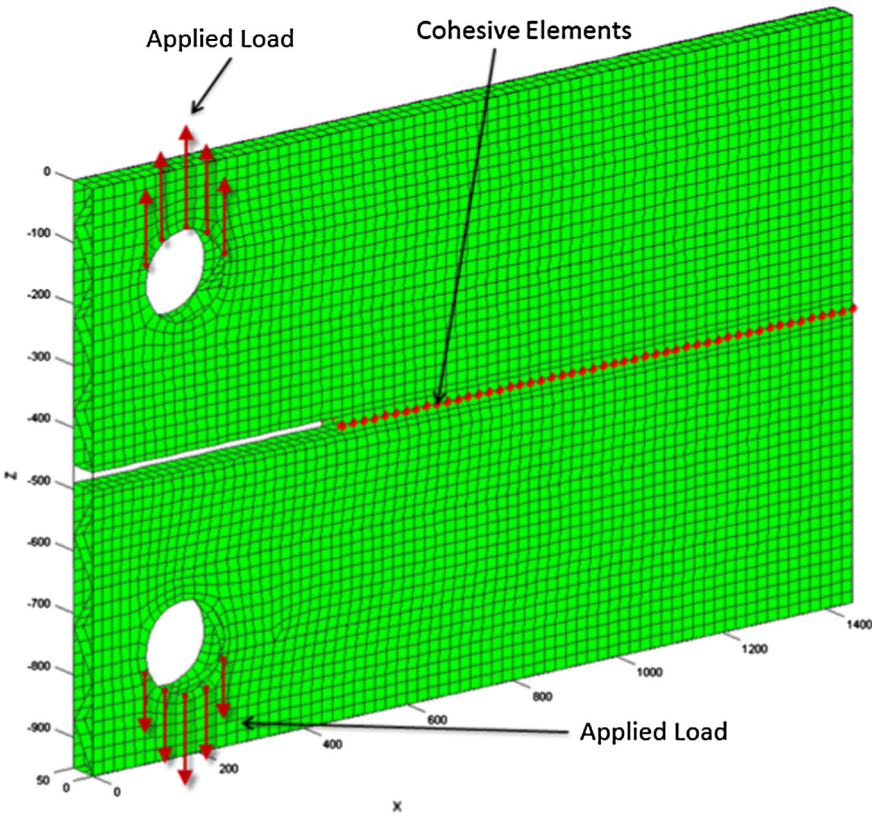

Fig. 11. Finite element model of welded AA 6061 extruded panel subjected to mode I tensile loading

cohesive zone with $\Gamma = \Gamma_{ss-weld} = 831$ kJ/m^2 and the traction-displacement relation derived from the coupon test in Fig. 7(c). This result for the load-load point displacement of the structure is compared the experimental result presented in Fig. 12. The agreement between the two curves is reasonably good but it is noted that the simulation overestimates the peak load by about 5%. This is not a large discrepancy, but based on the behavior discussed for mode I tearing of the large Al5083-H116 plate [42], one might also anticipate an x-dependence of the cohesive energy for the weld in the extruded panels with initial values that are lower than the steady-state value.

In order to quantify the x-dependence of the weld cohesive zone on the structural-scale calculation we employ an inverse identification of the cohesive energy prior to reaching the steady-state value obtained from the small-scale coupon calibration reported above. After the steady-state has been reached, the cohesive energy/area was assumed constant and equal to steady-state value obtained in the coupon test. By adjusting the cohesive energy step by step in the advancement of the crack, prior to reaching the steady state, the improved calibration, $\Gamma(\Delta x)$, shown in Fig. 13 is obtained which has been forced to asymptote to the steady-state value determined from the coupon test.

This second iteration on the calibration process generates the force-displacement behavior included in Fig. 12. In these simulations, the cohesive energy reduction was achieved by reducing the final separation δ^F while maintaining the peak traction and the overall shape of the traction-separation curve.

This second iteration of the calibration process to produce the x-dependent cohesive energy is based on the experimental data for the structure itself, apart from the steady-state limit, and thus the fact that it more accurately reproduces the behavior of the structure is hardly surprising. Additional structural tests with this plate thickness and weld-type are not available to put the second iteration to a critical test. However, the second iteration is useful to show that a reduction in the cohesive energy in the early stages of crack initiation and growth is likely, although only about 25% below the steady-state value obtained from the coupon test and thus far less than the reduction seen for the monolithic Al5083-H116 plate. Given the accuracy of the prediction for the simulations based on the x-independent cohesive energy with $\Gamma = \Gamma_{ss-weld} = 831$ kJ/m^2, one might well conclude that an improvement on the single coupon-based traction-separation law is unnecessary for the mode I tearing of the welded Al6061 plates. However, whether this conclusion holds for other undermatched welds remains to be determined by further studies.

Neither simulation captures the drop observed during the experiment starting at the displacement of ~14 mm, which was caused by the initiation of a second crack in the HAZ, away from the initial tip [50]. As already noted, the discretization level and the type of model used in the current investigation is not sufficient to capture the details of the second crack ini-

Please cite this article in press as: Woelke PB et al. A practical approach to modeling aluminum weld fracture for structural applications. Engng Fract Mech (2017), http://dx.doi.org/10.1016/j.engfracmech.2017.02.010

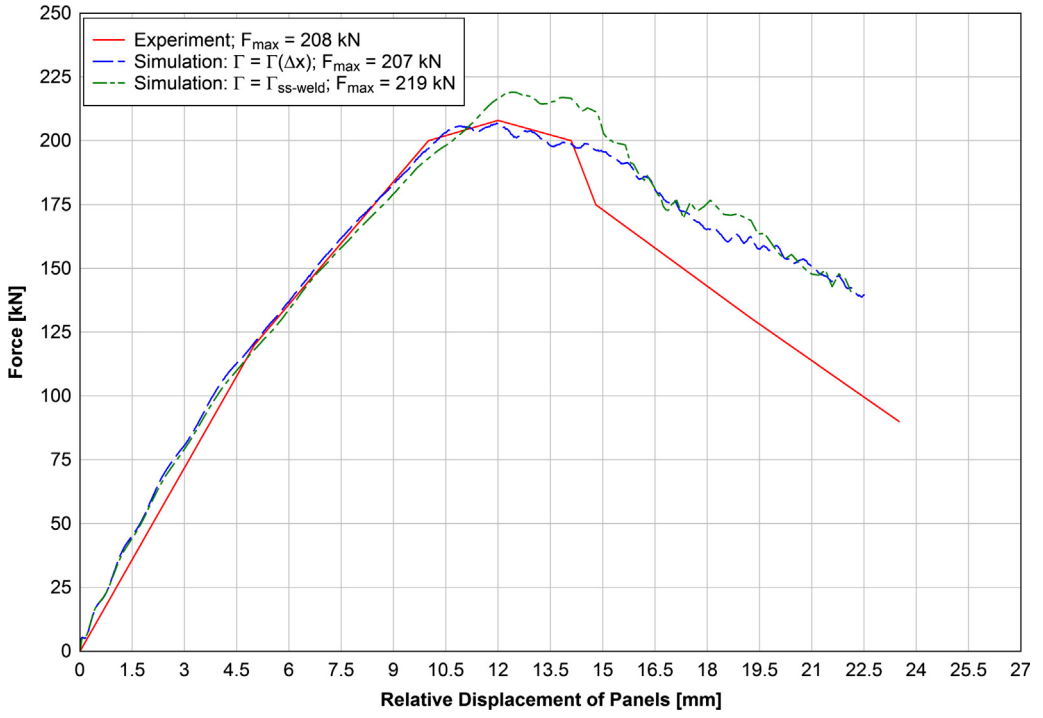

Fig. 12. Applied force vs. crosshead displacement measured in the experiment [50] and obtained by simulation with (i) cohesive energy/area dependent on crack advance $\Gamma(\Delta x)$ shown in Fig. 12 and, (ii) for a cohesive energy/area independent of crack advance with $\Gamma = \Gamma_{ss-weld}$ obtained from the coupon test.

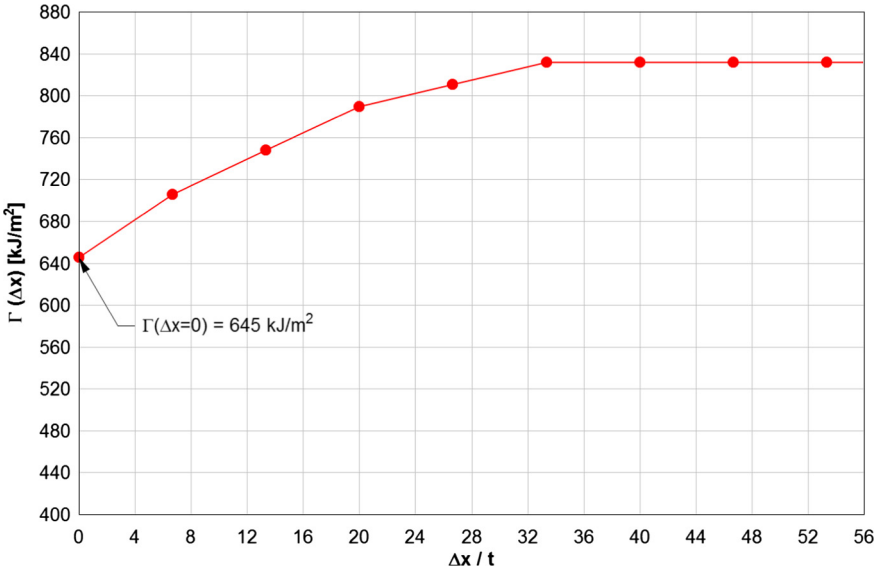

Fig. 13. Cohesive energy/area as a function of the distance ahead of the pre-crack Δx, normalized by the thickness of the face-sheet of the extrusion for mode I fracture of welded Al6061 extrusion tested in [50].

tiation in the HAZ. The discrepancy between the measured and calculated response after this crack is initiated is a little over 2% and, again, not very large, indicating that the second crack, possibly caused by a weld flaw, has not significantly affected the global force-displacement response of the panel. A more dramatic effect could however be observed if a weld flaw (e.g. large void) caused premature fracture initiation and propagation. The effects of weld flaws that depend on the welding process and quality control require further investigation that is beyond the scope of this paper.

Please cite this article in press as: Woelke PB et al. A practical approach to modeling aluminum weld fracture for structural applications. Engng Fract Mech (2017), http://dx.doi.org/10.1016/j.engfracmech.2017.02.010

We again emphasize that the results shown in Figs. 12 and 13 were obtained with a relatively coarse finite element model utilizing shell elements that are large compared to the plate thickness together with an independently calibrated cohesive zone, at least for the x-independent zone. As previously discussed, the main purpose of this work is to provide a simple and systematic approach to modeling fracture of undermatched welds for large-scale industrial applications in support of the design process. In this context, the agreement between the simulated and measured force-displacement response, even for the position-independent cohesive zone (i.e. $\Gamma = \Gamma_{ss-weld}$) far exceeds the typical level of accuracy achieved today in large-scale structural simulations performed in support of design of structures.

One of the possible reasons for this weak x-dependence of the cohesive energy for the welded plate structure (compared to the unwelded Al5083-H116 plate in [42]) is a very large notch radius, i.e. $\sim 4.5t$, where t is the face-sheet thickness of the extrusion. Another possibility is that the low level of constraint at the notch tip for thin sheets ($t = 3.2$ mm) combined with the low yield stress of the weld material and HAZ allow neck development and extensive plastic dissipation at the notch tip almost as soon as the crack begins to advance. Whether the weak R-curve behavior of the cohesive zone seen for the welded Al6061 extruded panel turns out to be the rule rather than the exception for other undermatched welded structures will be important to establish.

Another interesting observation can be made by comparing the steady-state cohesive energy/area ($\Gamma_{ss-weld} = 831$ kJ/m^2) obtained for the weld/HAZ of the Al 6061 plate with thickness $t = 3.2$ m with that of the analogous value obtained for the unwelded, 10 mm thick Al5083-H116 plate ($\Gamma_{ss} = 1175$ kJ/m^2). Since the steady-state cohesive energy/area is expected to depend nearly linearly on plate thickness, due to the fact that the neck height scales with thickness as discussed in [22], the weld/HAZ steady-state energy for a 10 mm plate, would be expected to be approximately three times that for the thinner welded plate, all other things being equal. This is clearly not the case—the cohesive energy of the much thinner welded plate is almost the same as that of the unwelded plate that is three times thicker, albeit the materials are not the same. What this does indicate is that the weld/HAZ material, while significantly weaker than the base material, is remarkably tough, owing to the significant ductility increase and the width of the heat affected region of the weld. Although the increased toughness is important, the small strength of the weld/HAZ causes plastic strain to be confined to the weld/HAZ with little or no plasticity outside this region, reducing the overall plastic dissipation. This is clearly shown in the equivalent plastic strain contour plot in Fig. 14. In the initial phase of propagation, plasticity is confined to cohesive zone only. When the crack approaches the end of the plate, significant bending stress is induced in the plate which causes compression near the free edge and additional plastic straining (outside the cohesive zone) near the crack tip. The extent of this additional plastic zone is still relatively small and confined to the immediate vicinity of the weld. By contrast, in the case of the unwelded Al5083-H116 plate, the majority of plastic dissipation (~66%) occurred outside the cohesive zone [42].

The above discussion suggests that modifications of the welding process for aluminum (as well as analysis and design methodologies) may be possible, to improve performance of the welded aluminum structures. One possible avenue is modifying the extent of the HAZ to produce more plastic dissipation in the cohesive zone and thus higher overall toughness of the structure.

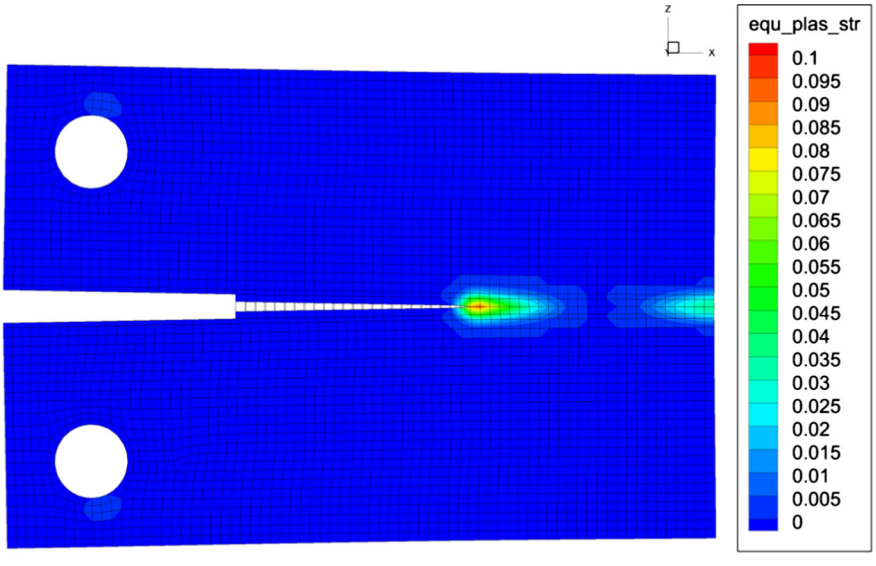

Fig. 14. Equivalent plastic strain contours for mode I fracture simulation of welded Al6061 extrusion.

Please cite this article in press as: Woelke PB et al. A practical approach to modeling aluminum weld fracture for structural applications. Engng Fract Mech (2017), http://dx.doi.org/10.1016/j.engfracmech.2017.02.010

5. Conclusions and future work

While use of aluminum alloys as structural material has a long history, recent efforts to reduce the weight of various structural systems (e.g. cars, aircraft, ships, trains, pipelines) has led to renewed interest in structural aluminum, mainly due to its low density and corrosion resistance. The light-weighting initiatives have resulted in multiple structural platforms that need to resist loads which can cause fracture and failure. This motivates research efforts aimed at new and effective analysis and design methodologies for large-scale welded aluminum structures.

A simple, effective method to predict ductile fracture in welded aluminum structures (WALFRAM - Welded Aluminum Fracture Modeling) using large shell elements and a cohesive zone has been proposed and evaluated here. The main focus of this paper is on mode I tensile fracture in large-scale welded aluminum structures with significant undermatching of the welds and HAZ. The simplest calibration process of the cohesive traction-separation relation, which represents the weld and HAZ, is performed based on a tensile test of a welded aluminum coupon for a plate of the same thickness. Appropriateness of the simple welded coupon geometry to represent behavior of linear undermatched weld, stems from the fact that the longitudinal constraint (in the weld direction) prevents deformation parallel to the weld. This causes localization through the thickness with a localized neck perpendicular to the loading direction. Thus, the calibration process is based on the specimen geometry that forces plane strain behavior, with the zero strain along the weld (as opposed to the thickness direction). The effectiveness of the proposed methodology in predicting mode I fracture in undermatched aluminum welds is demonstrated. Since the approach relies on localization of plasticity in the weld and HAZ, it will generally not be applicable for welded joints that are not undermatched, although a study of mode I tearing of unwelded plates [42] suggests that a similar approach can be effective with these other welds as well. On the other hand, the proposed approach is not limited to aluminum welds only, i.e. it will be equally effective for all undermatched linear welded joints under mode I loading (e.g. martensitic steels).

Several key areas of further research have been identified. They include development and validation of the mixed-mode (mode I-II-III) cohesive zone formulation that would allow for fracture mode interaction while maintaining simplicity of the calibration process. More research is also needed to understand the crack growth resistance behavior, where the crack initiates from the blunt notch in the weld/HAZ. While the cohesive zone for the welded plates in this study can be taken to be x-independent, to a good approximation, it does not seem to be widely appreciated that this may not be adequate for all problems, as illustrated in [42]. Another important area of investigation is the welding process itself, which may lead to characterization of the weld flaw distribution as well as reduction of the flaw frequency through adequate quality control. In addition, certain modifications of the welding process (e.g. increasing the extent of the HAZ) could possibly lead to better performance of welded aluminum structures. Investigation of these challenges and development of effective solutions could lead to significant improvements in the process of analysis, design and construction of large-scale welded aluminum structures.

Acknowledgements

The support of the Office of Naval Research: Dr. Paul Hess (Contract No. N00014-10-M-0252) is gratefully acknowledged. The authors also gratefully acknowledge technical assistance of Dr. Kim Nielsen (Technical University of Denmark) and William Hoffman (Naval Surface Warfare Center Carderock) who offered numerous valuable suggestions and Dr. Frank Zok (University of California at Santa Barbara) who performed experimental tests under a separate contract from NSWCCD, in collaboration with Dr. Ken Nahshon. The test data is given in Fig. 3.

References

[1] Anvari M, Scheider I, Thaulow C. Simulation of dynamic ductile crack growth using strain-rate and triaxiality-dependent cohesive elements. Eng Fract Mech 2006;73:2210–28.
[2] Baker H. Properties and selection: nonferrous alloys and pure metals. In: Metals handbook. American Society of Metals; 1979.
[3] Banik J, Gerber T, Graff S, Horstmann J, Koyer M, Lenze F, Liesner J, Middelhauve O, Mura J, Sikora S, Vives Diaz N. Hot Forming in the Automotive Industry. Processes, materials, coatings. ThyssenKrupp Steel Europe AG; 2013.
[4] Cavalli MN, Thouless MD, Yang QD. Cohesive-zone modelling of the deformation and fracture of spot-welded joints. Fatigue Fract Eng Mater Struct 2005;28:861–74.
[5] Hachez F. Experimental and numerical investigation of the thickness effect in the ductile tearing of thin metallic plates PhD Thesis. Universite Catholique de Louvain; 2008.
[6] Hao S, Schwalbe KH, Cornec A. The effect of yield strength mis-match on the fracture analysis of welded joints: slip-line field solutions for pure bending. Int J Solids Struct 2000;37(39):5385–411.
[7] Kissel JR, Ferry RL. Aluminum structures. A guide to their specification and design. 2nd ed. John Wiley & Sons; 2002. ISBN 0-471-01965-8.
[8] Kõrgesaar M, Romanoff J. Influence of mesh size, stress triaxiality and damage induced softening on ductile fracture of large-scale shell structures. Marine struct 2014;38:1–17.
[9] Li H, Chandra N. Analysis of crack growth and crack-tip plasticity in ductile materials using cohesive zone models. Int J Plast 2003;19:849–82.
[10] Liu C, Northwood DO, Bhole SD. Tensile fracture behavior of CO_2 laser beam welds of 7075–T6 aluminum alloy. Mater Des 2004;25:573–7.
[11] Liu HJ, Fujii H, Maeda M, Nogi K. Tensile properties and fracture locations of friction-stir-welded joints of 2017–T351 aluminum alloy. J Mater Process Technol 2003;142:692–6.
[12] Matusiak M. Strength and ductility of welded structures in aluminum alloys Ph.D. Thesis. Department of Structural Engineering, Norwegian University of Science and Technology; 1999.
[13] Mazzolani FM. Aluminum alloy structures. 2nd ed. E&FN Spon; 1995. ISBN 0 419 17770 1.
[14] Nahshon K, Zok F. Private communications – Contract No. N00167-09-P-0331; 2009.

Please cite this article in press as: Woelke PB et al. A practical approach to modeling aluminum weld fracture for structural applications. Engng Fract Mech (2017), http://dx.doi.org/10.1016/j.engfracmech.2017.02.010

[15] Nahshon K, Hutchinson JW. Modification of the Gurson Model for shear failure. Eur J Mech A/Solids 2008:1–17.
[16] Needleman A. An analysis of decohesion along an imperfect interface. Int J Fract 1990;42:21–40.
[17] Negre P, Steglich D, Brocks W, Kocak M. Numerical simulation of crack extension in aluminum welds. Comput Mater Sci 2003;28:723–31.
[18] Negre P, Steglich D, Brocks W. Crack extension in aluminum welds: a numerical approach using the Gurson-Tvergaard-Needleman model. Eng Fract Mech 2004;71:2365–83.
[19] Nielsen KL. Ductile damage development in friction stir welded Aluminum (AA2024) joints. Eng Fract Mech 2008;75(10):2795–811.
[20] Nielsen KL, Tvergaard V. Effect of a shear modified gurson model on damage development in a FSW tensile specimen. Int J Solids Struct 2009;46:587–601.
[21] Nielsen KL. Predicting failure response of spot welded joints using recent extensions to the Gurson model. Comput Mater Sci 2010;48:71–82.
[22] Nielsen KL, Hutchinson JW. Cohesive traction-separation laws for tearing of ductile metal plates. Int J Impact Eng 2011;48:15–23.
[23] Ortiz M, Pandolfi A. Finite-deformation irreversible cohesive elements for three-dimensional crack-propagation analysis. Int J Numer Methods Eng 1999;44:1267–82.
[24] Rashind MM, Tvergaard V. Crack trajectory near a weld: Modeling and simulation. Eng Fract Mech 2008;75:560–70.
[25] Reynolds AP, Duvall F. The welding journal research supplement, vol. 78(10); 1999. p. 355–60.
[26] Scheider I, Brocks W. Cohesive elements for thin-walled structures. Comput Mater Sci 2006;37:101–9.
[27] Sills RB, Thouless MD. The effect of cohesive-law parameters on mixed-mode fracture. Eng Fract Mech 2013;109:353–68.
[28] Simonsen BC, Törnqvist R. Experimental and numerical modelling of ductile crack propagation in large-scale shell structures. Mar Struct 2004;17:1–27.
[29] Sutton MA, Reynolds AP, Yang B, Taylor R. Mode I fracture and microstructure for 2024–T3 friction stir welds. Mater Sci Eng 2003;A354:6–16.
[30] Tabor D. The physical meaning of indentation and scratch hardness. Br J Appl Phys 1956;7:159–66.
[31] Tvergaard V, Hutchinson JW. The relation between crack growth resistance and fracture process parameters in elastic-plastic solids. J Mech Phys Solids 1992;40:1377–97.
[32] Tvergaard V, Hutchinson JW. Effect of strain-dependent cohesive zone model on predictions of crack growth resistance. Int. J. Solids Struct 1996;33:3297–308.
[33] Tvergaard V, Hutchinson JW. Mode III effects on interface delamination. J Mech Phys Solids 2008;56:215–29.
[34] Volokh KY. Comparison between cohesive-zone models. Commun Numer Methods Eng 2004;20:845–56.
[35] Voyiadjis GZ, Woelke P. General non-linear finite element analysis of thick plates and shells. Int. J. Solids Struct 2005;43(7–8, 1):2209–42.
[36] Voyiadjis GZ, Woelke P. Elasto-plastic and damage analysis of plates and shells, 2008. Springer-Verlag; 2008. ISBN: 978-3-540-79350-2.
[37] Wadley HNG, Børvik T, Olovssond L, Wetzela JJ, Dharmasena KP, Hopperstad OS, et al. Deformation and fracture of impulsively loaded sandwich panels. J Mech Phys Solids 2013;61(2):674–99.
[38] Wang T, Hopperstad OS, Larson PK, Lademo O-G. Evaluation of a finite element modeling approach for welded aluminum structures. Comput Struct 2006;84:2016–3032.
[39] Wang T, Hopperstad OS, Lademo O-G, Larsen PK. Finite element modeling of welded aluminum members subjected to four-point bending. Thin-Walled Struct 2007;45:307–20.
[40] Woelke P, Abboud N. Modeling fracture in large scale shell structures. J Mech Phys Solids 2012;60(12):2044–63.
[41] Woelke P, Shields MD, Abboud NN, Hutchinson JW. Simulations of ductile fracture in the idealized ship grounding scenario using phenomenological damage and cohesive zone models. Comp Mater Sci 2013;80:79–95.
[42] Woelke PB, Shields MD, Hutchinson JW. Cohesive zone modeling and calibration for mode I tearing of large ductile plates. Eng Fract Mech 2015;147:293–305.
[43] Woelke PB, Rutner MP, Shields MD, Rans C, Alderliesten R. Finite element modeling of fatigue in fiber-metal laminates. AIAA J 2015;53:2228–36.
[44] Woelke P, Voyiadjis GZ, Perzyna P. Elasto-plastic finite element analysis of shells with damage due to microvoids. Int J Num Meth Eng 2006;68 (3):338–80.
[45] Woelke P, Chan KK, Daddazio R, Abboud N. Stress resultant based elasto-viscoplastic thick shell model. Shock Vib 2012;19:477–92.
[46] Woelke P, Chan KK, Daddazio R, Abboud N, Voyiadjis GZ. Analysis of shear flexible layered isotropic and composite shells by EPSA. Shock Vib 2012;19:459–75.
[47] Woelke P, Chan KK, Daddazio R, Abboud N. Stress-resultant based elasto-viscoplastic thick shell model. Shock Vib 2012;19:477–92.
[48] Yang QD, Thouless MD. Mixed-mode fracture analyses of plastically-deforming adhesive joints. Int J Fract 2001;110:175–87.
[49] Zheng L, Petry D, Wierzbicki T, Rapp H. Mode III fracture of a large-scale welded extruded aluminum panel. Thin-Walled Struct 2008;46:1262–73.
[50] Zheng L, Petry D, Rapp H, Wierzbicki T. Mode I fracture of large-scale welded thing-walled AA 6061 extruded panels. Thin-Walled Struct 2009;47:375–81.
[51] Zheng L, Petry D, Rapp H, Wierzbicki T. Characterization of material and fracture of AA6061 butt weld. Thin-Walled Struct 2009;47:431–41.
[52] Zheng L, Petry D, Rapp H, Wierzbicki T. Fracture prediction in 4-point bending of an extruded aluminum panel. Thin-Walled Struct 2005;43:565–90.
[53] Zhou B, Thouless MD, Ward SM. Determining mode-I cohesive parameters for nugget fracture in ultrasonic spot welds. Int J Fract 2005;136:309–26.
[54] Zhou B, Thouless MD, Ward SM. Predicting the failure of ultrasonic spot welds by pull-out from sheet metal. Int J Solids Struct 2006;43:7482–500.

Please cite this article in press as: Woelke PB et al. A practical approach to modeling aluminum weld fracture for structural applications. Engng Fract Mech (2017), http://dx.doi.org/10.1016/j.engfracmech.2017.02.010